Real-Time Characterization of Period-Doubling Dynamics in Uniform and Dispersion Oscillating Fiber Ring Cavities

Florent Bessin, François Copie, Matteo Conforti, Alexandre Kudlinski, Arnaud Mussot, Stefano Trillo

Real time characterization of period-doubling dynamics in uniform and dispersion oscillating fiber ring cavities

Florent Bessin,* François Copie, Matteo Conforti, Alexandre Kudlinski, and Arnaud Mussot
Université Lille, CNRS, UMR 8523-PhLAM-Physique des Lasers Atomes et Molécules, F-59000 Lille, France

Stefano Trillo
Department of Engineering, University of Ferrara, Via Saragat, 44122 Ferrara, Italy
(Dated: October 4, 2019)

Modulational instability in passive optical resonators, the triggering mechanism of frequency comb and pulse train generation, is shown to exhibit transitions between regimes involving period-one (P1) versus period-two (P2) dynamical evolutions. The latter is a signature of parametric resonance occurring in the system, which can arise either from intrinsic cavity periodicity or from spatial modulation of the cavity parameters. We characterize the P1-P2 transition for both cases employing a fiber resonator where the intra-cavity fiber can be either uniform or dispersion modulated. The key element of our setup is a time lens which we exploit to resolve the temporal dynamics over successive round-trips, allowing crystal clear evidence of the existence of P1-P2 transitions for suitable changes of cavity parameters, as well as for the successful characterization of the relative temporal patterns. Our findings reveal new regimes where the averaged model known as Lugiato-Lefever equation turns out to be inadequate to explain the dynamics, whereas the results are correctly predicted and described on the basis of the full Ikeda map.

I. INTRODUCTION

The generation of frequency combs has attracted a lot of attention during the last decades since these ultra-precise optical rulers have a wealth of applications ranging from astrophysics, metrology, or spectroscopy to name a few [1, 2]. Also associated with formation of cavity solitons in time domain [3, 4], their generating mechanism relies on modulation instability (MI) which first initiates the exponential growth of two symmetric sidebands around the pump [5, 6]. Then, subsequent four-wave mixing processes lead to the generation of additional equidistant lines to eventually form ultra-broadband spectra which might reach an octave [7]. Characteristics of the frequency comb thus strongly depend on these early stages of formation and a perfect knowledge of the MI dynamics is essential to understand their formation in order to optimize their performances [8]. First observation of MI in passive resonators has been achieved by Coen and Haelterman [9] in an all fiber system. This seminal works has motivated further investigations aimed at understanding the complex and rich dynamics of MI processes that may arise beyond the basic configuration. More recent investigations have addressed passive fiber ring cavities in the weak dispersion regime [10–12], under-strong cavity driving to reach nonlinear shifts larger than 2π [7, 13–15], through polarization effects [16, 17] and in dispersion modulated cavities [18–21].

The common thread between these complex systems, compared to the basic configuration studied in Ref. [6, 9], is that new parametric resonances are excited [7, 10–16, 18–22]. The striking feature is not limited to the generation of new sets of frequencies but also to the modification of the whole behavior of the system. From a theoretical point of view, these new parametric resonances correspond to new eigenvalues of the system, that might be positive or negative, thus leading to temporal shifts of the output pattern from round-trip to round-trip [14, 20, 23, 24]. In modulationaly unstable systems, [5, 25] the output cavity pulse train can either be out of phase round-trip to the other, which is denoted as P2 regime or, conversely, in phase in the so-called P1 regime [20]. In particular the P2 regime turns out to be inherently associated with the parametric resonance phenomenon induced by system periodicity. However, different sources of periodicity such as the intrinsic periodicity associated with the cavity boundary conditions in a uniform cavity, or ad hoc introduced modulation of the cavity parameters (e.g. dispersion, nonlinearity, etc.) can have different impact on how the parametric resonance reflects itself into the onset of P2 regimes. To date, however, only indirect evidence of such phenomena have been reported through observation of spectral sideband generation (see [26] for a uniform cavity and [19, 27] for a cavity with modulation of dispersion). Conversely, the true assessment of P2 regimes by means of real-time observations over the time scale of the round-trip remains extremely challenging and has never been reported so far. The general importance of such type of measurement stands also on the fact that P2 regime is a well-known mechanism in nonlinear systems supporting bistable states, first predicted by Ikeda *et al.* [28], which was identified as a first step in a universal route to chaos. It has been observed in modulationaly stable passive fiber cavities [29–31] and investigated in active lasers in theory [32–34] and in experiments [35, 36].

In this paper, we report direct observations in the time domain of P1 and P2 regimes in both uniform and modulated passive fiber ring cavities. We implemented a time

* florent.bessin@univ-lille.fr

lens [37] which is a recent instrumentation developed to study in real time optical rogue waves [38, 39] or to characterize transient dynamics in active lasers [40]. This device based on space time duality [41] magnifies temporally the cavity output pulse train whose period lies in the picosecond scale to reach nanosecond duration that can be measured in real-time, round-trip to round-trip using high speed photodetectors. Thus, π or 2π shifts experienced by the output pulse train round-trip to round-trip can be observed and thus the nature of the regime, P1 or P2, identified. Moreover, we provide theoretical development to support these experimental observations.

The paper is organized as follows. In section II, a theoretical description of both uniform (section II B) and modulated cavities (section II C) is presented. We end up with parametric gain expressions which allow the description of the dynamics and to identify P1 and P2 regimes. In section III, experimental results are presented. First, the experimental setup used in both cavity configurations is described (section III A) followed by experimental results in a uniform passive fiber cavity (section III B 1) and a dispersion modulated one (section III B 2).

II. THEORETICAL INVESTIGATIONS

A. Governing equations

We consider a passive fiber ring cavity modeled by the following Ikeda map model [28]:

$$\frac{\partial E_n(z,t)}{\partial z} = \Big(-\frac{\alpha_f}{2} - i\frac{\beta_2(z)}{2}\frac{\partial^2}{\partial t^2} + i\gamma|E_n(z,t)|^2\Big)E_n(z,t) \tag{1}$$

$$E_{n+1}(0,t) = \rho E_n(L,t)\exp(i\Phi_0) + \theta E_{in}(t) \tag{2}$$

where Eq. (1) is the nonlinear Schrödinger equation (NLSE) that rules the propagation of the intra-cavity field E_n (respectively intra-cavity power $P = |E_n|^2$) during the n-th round-trip along the cavity of length L, in the reference frame moving at the wave group velocity. The parameters β_2, γ, and α_f are respectively the group velocity dispersion (GVD), the nonlinear coefficient and the fiber loss coefficient. Equation (2) accounts for the periodic boundary conditions imposed by the coupler at each round-trip, where ρ and θ are respectively the reflection and transmission coefficients of the coupler defined such that $\rho^2 + \theta^2 = 1$. Parameter E_{in} refers to the pump input field (respectively input-power $P_{in} = |E_{in}|^2$) and Φ_0 is the linear phase accumulated by the intra-cavity field over one round-trip. The cavity detuning δ_0 is defined such as $\delta_0 = 2k\pi - \Phi_0$, with k an integer, chosen such that the cavity detuning refers to the detuning of the pump frequency from the closest resonance of the cavity. Note that while it is often very convenient to investigate the dynamics of this system using a simplified model such as the Lugiato-Lefever equation (LLE) [5], this one is not valid for large values of the cavity detuning [10, 13, 15, 20]. Some of the results presented here were obtained outside the range of validity of this model which is thus not fully relevant for our study.

In the following, we first study the emergence of P1/P2 regimes by means of Floquet theory in the most simple cavity configuration: uniform fiber cavity. Then we will extend this analysis to dispersion a modulated fiber cavity.

B. Uniform fiber cavities

A schematic of the passive cavity is shown in Fig. 1(a) along with the evolution of the GVD over one cavity round-trip in Fig. 1(b). As detailed in Ref. [20], the dynamics of the system is well described by performing a linear stability analysis of the complete map system (Eq. (1-2)) using the method described in [9, 42]. We obtain a system of difference equations whose evolution is ruled by the product of the fundamental matrix calculated from linear stability analysis of Eq. (1) (at z=L) and rotation matrix owing to the boundary conditions (Equation (2)). As a result, the stability of this system depends on eigenvalues of the product of these two matrices. For modulus of eigenvalues larger than unit, the steady-state cw solution is unstable with respect to harmonic perturbation, which initially grows exponentially. Assuming that fiber propagation losses are small relative to coupling losses, the overall cavity losses can be approximated by $\alpha = 1 - \rho\exp(-\alpha_f/L)$ which leads to eigenvalues expressed as [20]:

$$\lambda_\pm = (1-\alpha)\left[\Psi \pm \sqrt{\Psi^2 - 1}\right] \tag{3}$$

where

$$\Psi = [\cos(\mu L)\cos(\Phi) - \kappa\sin(\mu L)\sin(\Phi)] \tag{4}$$

Parameter $\Phi = \gamma LP + \Phi_0$ refers to the total phase accumulated over a round-trip, while:

$$\mu = \sqrt{\frac{\beta_2^2\Omega^4}{4} + \beta_2\gamma P\Omega^2} \tag{5}$$

to the standard MI gain with Ω the pulsation of the perturbation, and $\kappa = (\beta_2\Omega^2/2 + \gamma P)/\mu$. It can be easily checked that unstable eigenvalues (i.e. $|\lambda| > 1$) appear only for $|\Psi| > [1 - \alpha + 1/(1-\alpha)]/2$ which leads to real eigenvalues that can be expressed as $\lambda = |\lambda|e^{im\pi}$ with m integer. As a consequence, an infinite number of frequencies can be destabilized, each of them being associated to a parametric resonance of the system. We introduce λ' that corresponds to the eigenvalue $\lambda_\pm$ with the highest modulus, hence the complex gain turns out to be $\ln(|\lambda'|)/L + im\pi/L$. Two distinct cases appear depending on the value of m: (i) For m even (i.e. $\lambda' > 1$) the initial perturbation grows exponentially (with growth rate $g_{uniform} = \ln(|\lambda'|)/L$) following a P1 dynamics. (ii) For m odd (i.e. $\lambda' < -1$), the perturbation changes sign at every round-trip which is characteristic of a P2 dynamics. A clear-cut evidence of this behavior is the π phase shift

experienced by the temporal pattern from round-trip to round-trip as opposed to the P1 case. An overview of the behavior of the system in terms of P1/P2 regimes can be obtained by looking at the maximum gain value calculated from the growth rate $g_{uniform}$ in the (δ_0, P) plane (See Fig. 1(c)). This representation is relevant since it allows a comprehensible description of the dynamics of the systems, and these parameters correspond to those easily accessible from an experimental point of view. In this work we focus our attention on the case of normal dispersion that reveals more easily the striking features of the system. Indeed, cavities operating in the anomalous dispersion regime are known to exhibit MI under a rather large range of parameters which is likely to hinder the observation of a competition between P1 and P2 dynamics. Figure 1(c) shows that the system exhibits an alternation of narrow and broad instability tongues associated to P1 and P2 dynamics respectively. As soon as the pump power is above a certain threshold that depends on the amount of losses, the system might enter in one of the unstable region. We can point out that this mapping is necessarily 2π-periodic with respect to δ_0, owing to the periodicity of the linear resonances of the cavity. Accordingly, the most noteworthy features of the system can be illustrated by considering only two scenarios at MI cavity threshold: the first one, where the nonlinear phase is close to zero, and the second one, where the phase is close to π. These two cases have been called resonant and anti-resonant cases in Ref. [9], respectively. Nevertheless, well above MI threshold this denomination is not relevant anymore. Indeed, the nonlinear phase shift ($\Phi_{NL} = \gamma LP$) induces a displacement of resonance peaks of several radians, thus we shall use in this paper the denomination positive and negative detuning (δ_0) in order to correctly identify the different scenarios.

First, let's consider the cavity operating on positive detuning. As an example we set the cavity detuning to $\delta_0 = 1.44$ rad, indicated by the vertical green line in Fig. 1(c). For this value of detuning, the system is bistable and two distinct instability tongues can be accessed depending on the intra-cavity power. For a better understanding, we plot in Fig. 1(d) the corresponding steady-state curve function:

$$P = \frac{\theta^2 P_{in}}{1 + (1-\alpha)^2 - 2(1-\alpha)\cos(\Phi)} \qquad (6)$$

in the (P_{in}, P) plane (green curve). The dashed line between the knees of this S-shaped curve delimits the 'unconditionally unstable domain' regarding continuous wave while blue lines indicate unstable states as regards unstable domains in Fig. 1(c). With a pump power above the threshold for the first instability tongue on the lower-branch of the steady-state curve ($P_A = 1.56$ W, point A in Fig. 1(c), (d)), a pulse train stable from one round-trip to the other can be excited and thus corresponds to a P1 dynamics. This lower-branch is known to be modulationaly unstable if $\Delta > 4.25$, with $\Delta = \delta_0/\alpha$, and is linked to the so-called Turing instability [43, 44]. By increasing the intra-cavity power to $P_B = 5.84$ W (point

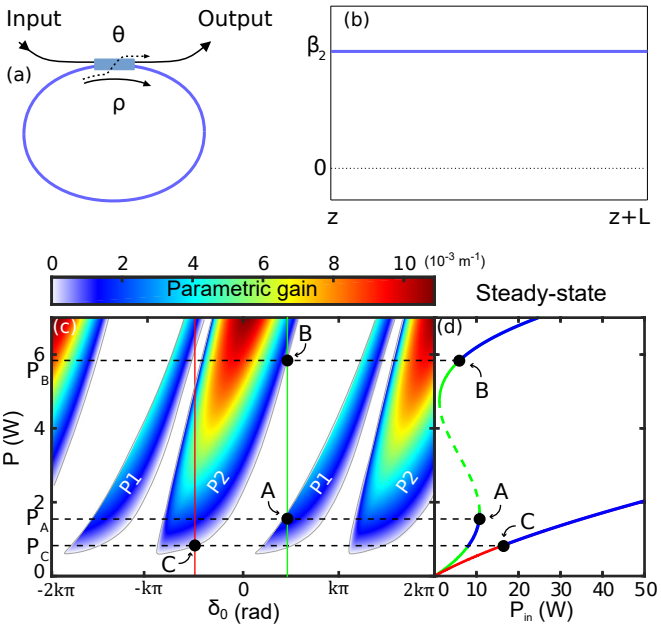

FIG. 1. (a) Schematic of the cavity. (b) GVD evolution over one cavity round-trip. (c) 2D-map of the maximum parametric gain in the plan (δ_0, P). (d) Steady-state curves of the cavity for $\delta_0 = 1.44$ rad (green curve) and $\delta_0 = -1.6$ rad (red curve), blue parts stand for the region where P1 and P2 regimes can be excited. Parameters: $\beta_2^{DSF} = 9$ ps^2.km^{-1}, L=120.6 m, $\gamma = 2.5$ W^{-1}.km^{-1}, cavity losses $\alpha = 0.165$.

B in Fig. 1(c), (d)), the system switches to the upper-branch of the steady-state curve (See Fig. 1(d)) and falls within another parametric instability tongue that is associated to a P2 dynamics. Let's point out that such a behavior could not be anticipated using the Lugiato-Lefever model, which predicts a steady-state for the system [18, 25, 43].

Second the cavity detuning is set to negative value. For example, $\delta_0 = -1.6$ rad, vertical red line in Fig. 1(c)). The steady-state curve for this detuning is plotted in Fig. 1(d) (red curve) and we notice that the P2 instability can be accessed for a lower intra-cavity power ($P_C = 0.83$ W, point C in Fig. 1(c), (d)). At this large negative detuning value, it is also possible to switch on P1 tongue with a huge increase of pump power to $P_{in} \approx 180$ W, which is not accessible with standard experimental equipments.

C. Dispersion modulated fiber cavities (DMF)

A similar mathematical approach can be applied to modulated cavities [20]. For the sake of simplicity we focus on the specific case where only the GVD is modulated along the cavity length with a piecewise constant dispersion profile, this one corresponding to almost all realistic fiber optics configurations [45]. However, similar behavior is expected to be observed when varying any other cavity parameter regardless of the exact modulation format [22, 46]. A schematic of the cavity is shown in Fig. 2(a) along with the GVD evolution $\beta_2(z)$ (Fig.

2(b)). We consider here a cavity built out of two pieces of uniform fibers of length L_a and L_b with GVD coefficients $\beta_{2,a}$ and $\beta_{2,b}$ respectively. This corresponds to the simplest configuration for which the period of dispersion ($\Lambda = L_a + L_b$) is equal to the cavity length L. We define the ratio between these lengths $N = \frac{L}{\Lambda}$, thus $N = 1$ in this example. This value can be arbitrarily larger and for the sake of generality, theoretical investigations had been performed for any integer values of N. As the previous studied case of uniform cavities, we investigate the dynamics of this system thanks to a linear stability analysis of the complete map system (Eq. (1-2)). We obtain a system of difference equations whose evolution is ruled by the product of the fundamental matrices of each uniform fiber calculated from Eq. (1) and rotation matrix owing to the boundary conditions Equation (2). The stability of this system depends on eigenvalues of the product of these matrices which can be expressed in the form of Eq. (3) over a period Λ where now:

$$\Psi = [\cos(\mu_a L_a)\cos(\mu_b L_b) - \sigma_1 \sin(\mu_a L_a)\sin(\mu_b L_b)] \times \cos(\Phi) - \sin(\Phi)\times [\sigma_2 \sin(\mu_a L_a)\cos(\mu_b L_b) + \sigma_3 \cos(\mu_a L_a)\sin(\mu_b L_b)] \quad (7)$$

with:

$$\sigma_1 = \frac{(\beta_{2,a}\mu_a)^2 + (\beta_{2,b}\mu_b)^2}{2\beta_{2,a}\beta_{2,b}\mu_a\mu_b} \quad (8)$$

$$\sigma_{2/3} = \frac{(\beta_{2,a/b}\Omega^2)^2 + 4\mu_{a/b}^2}{4\mu_{a/b}\beta_{2,a/b}\Omega^2} \quad (9)$$

The parameter $\mu_{a/b} = \sqrt{(\beta_{2,a/b}^2\Omega^4)/4 + \beta_{2,a/b}\gamma P\Omega^2}$ refers to the standard MI gain with Ω the pulsation of the perturbation for fibers a and b. Unstable eigenvalues appear for the same condition as in uniform cavities, and again, they are always real. Consequently, introducing λ' that corresponds to the eigenvalue $\lambda_\pm$ with the highest modulus, the complex gain over a cavity round-trip (i.e. over N period Λ) reads as $N\ln(|\lambda'|)/\Lambda + iNm\pi/\Lambda$ with m integer. From this expression, contrary to the case of uniform cavity studied in section II B, P1/P2 regimes are not associated only to the order m but also to the number of dispersion periods forming the cavity N. Indeed for m odd and an odd number of dispersion periods, perturbations experience an exponential growth with a growth rate $g_{DMF} = N\ln(|\lambda'|)/\Lambda$ and a π phase shift (P2 regime) at each round-trip while in all other cases, there is no π phase shift (P1 regime). A summary of all the combination (N, m) is presented in Table I.

		$N = L/\Lambda$	
		even	odd
m	even	P1	
	odd	P1	P2

TABLE I. Conditions under which parametric instabilities exhibit a P1 or P2 dynamics in dispersion modulated cavities.

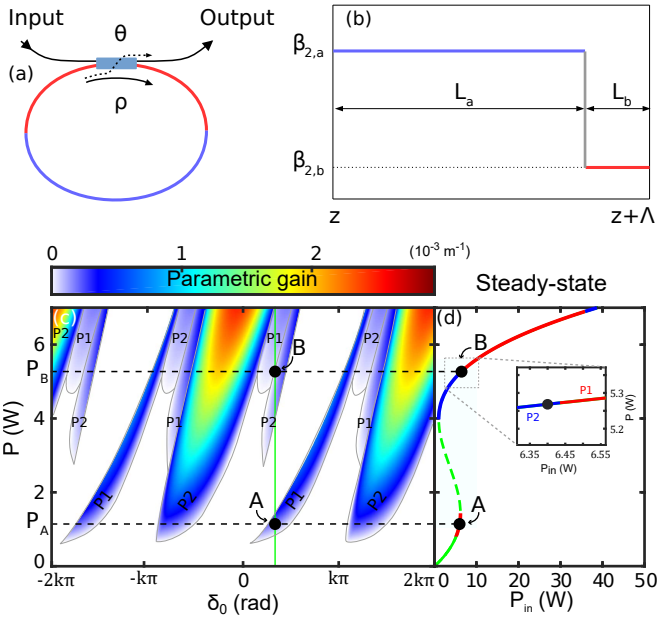

FIG. 2. (a) Schematic of the cavity. (b) GVD evolution over one cavity round-trip. (c) 2D-map of the maximum parametric gain in the plan (δ_0, P). (d) Steady-state curve of the cavity for $\delta_0 = 1.1$ rad (green curve), red (blue) parts stand for the region where P1 (P2) regime can be excited, inset: zoom on B point. Parameters: $\beta_2^{SMF-28} = -19$ ps^2.km^{-1}, $L^{SMF-28} = 1.6$ m, $\beta_2^{DSF} = 2$ ps^2.km^{-1}, $L^{DSF} = 48.1$ m, $\gamma = 5.5$ W^{-1}.km^{-1}, cavity losses $\alpha = 0.157$, $L = \Lambda$

.

For the sake of simplicity, we focus on the case where $N = 1$, which is the easiest configuration to implement experimentally [19, 21, 27, 47, 48].

Similarly to the uniform cavity studied in Section II B, Fig. 2(c) showcases a 2D-map in the (δ_0, P) plane of the maximum gain value calculated from the growth rate g_{DMF}. Many parametric instability tongues appear characterized either by a P1 or P2 dynamics. We work in a range of detuning regime which allows to observe Turing and Faraday instabilities, that is to say P1 and P2 dynamics respectively, by simply tuning the pump power keeping a constant cavity detuning [19, 21, 27, 47]. The cavity detuning is set to $\delta_0 = 1.1$ rad (marked by a vertical green line in Fig. 2(c)) that leads to a normalized cavity detuning $\Delta = 7$ large enough to allow the Turing instability to reach a steady-state [44]. By setting the pump power above the cavity threshold ($P_A = 1.14$ W, point A) Turing instability is excited on the lower-branch of the steady-state curve (Fig. 2(d)) and is characterized by a P1 dynamics. The upper-branch can be reached through an increase of the pump power up to $P = 5.27$ W (point B). The system has then switched to another instability tongue which is characterized by a P2 dynamics (see inset Fig. 2(d)). The Faraday mechanism is known to be at the origin of multiple tongues of instability [49], and a further increase of the pump power would bring the system to a regime where another parametric instability tongue can be excited, characterized by a P1 dynamics.

As expected from previous theoretical works, Turing instability is always ruled by a P1 type instability while the Faraday one can be either P1 or P2.

III. EXPERIMENTAL INVESTIGATIONS

In this section we experimentally study the emergence of P1 and P2 regimes in the temporal domain in uniform and dispersion modulated cavities.

A. Experimental setup

The experimental setup is depicted in Fig. 3. It is similar to those used in [12, 21]. It consists of a passive fiber cavity either made of a uniform or a dispersion modulated fiber (see parameters listed in Figs. 1 and 2) closed by a 90/10 coupler. In the uniform cavity, the coupler is made of the same fiber than the whole cavity (a specially designed dispersion shifted fiber, $\beta_2^{DSF} = 9 \ \ ps^2/km$) to get a perfectly uniform cavity while for the dispersion modulated cavity it is a standard SMF-28 fiber. To drive the cavity, a train of square pulses of 1 ns duration is used. It allows to prevent from Brillouin scattering and to get high peak power to trigger the MI process. These pulses are generated from a continuous wave (cw) laser at 1550.5 nm chopped by an electro-optical modulator (EOM). The repetition rate is set to match with the repetition rate of the cavity to get one pulse per round-trip. Pulses are then amplified by an erbium-doped fiber amplifier (EDFA) and pass through a thin filter (BPF, 1 nm width) to remove the amplified spontaneous emission (ASE) in excess. Pump pulses are launched into the cavity in the anti-clockwise (blue arrows) direction while a fraction of the output power of the EOM is launched in the clockwise direction (green arrows). This sample is used to stabilize the cavity to small external perturbations thanks to a feedback loop system (proportional-intergral-derivative-controller which finely tunes the cw laser wavelength) [11, 19, 26]. The cavity output is studied by means of an optical spectrum analyzer (OSA) and a commercial time lens system (Picoluz ultrafast temporal magnifier, Thorlabs) based on the results published in Ref. [37]. The time lens system is pumped by a femtosecond laser centered at 1570 nm. This laser will serve as a reference clock for the rest of the setup to get a perfect synchronization between all laser pulses involved in the experimental system. The cavity length is carefully adjusted with a fiber stretcher in order that the laser repetition rate of the time lens pump about 100 MHz is an exact multiple of the cavity repetition rate (typically 59 times for the uniform cavity and 24 times for the modulated cavity). The magnified signal (magnified factor of 57) is recorded by a fast oscilloscope and photodiode (70 GHz bandpass each). However we added a fiber Bragg grating (FBG), used in transmission, and placed just before the time lens in order to lower the power of the central component. It allows to reduce the relative amplitude of the continuous wave component compared to the modulated ones in the time domain, in order to record the periodic temporal patterns. Thanks to this method we recorded the temporal waveforms with approximately 300 fs of resolution over a window of 50 ps. This resolution is short enough to record MI temporal patterns which period of modulation lies in the picosecond range.

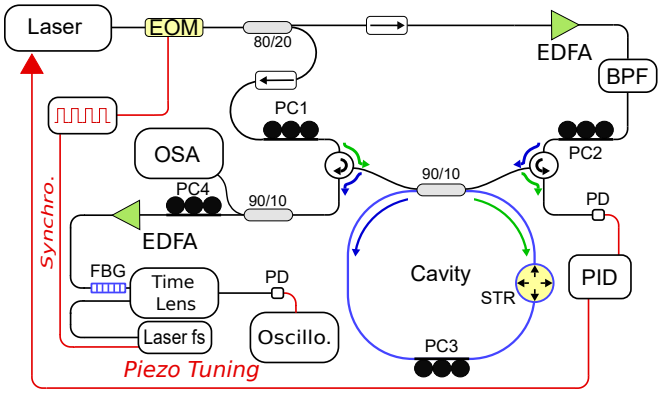

FIG. 3. Experimental setup. PC, polarization controller; STR, stretcher; PD, photo-detector; EOM, electro-optic modulator; OSA, optical spectrum analyser; EDFA, erbium-doped fiber amplifier; BPF, band-pass filter; PID, proportional-integral-derivate controller; Laser fs, femtosecond laser; Oscillo., oscilloscope; FBG, fiber Bragg gratting

B. Experimental results

Experimental results have been performed in both uniform and modulated cavities to observe the P1-P2 transition described in theory and marked by A, B and C points in Fig. 1(c-d) and by A and B points in Fig. 2(c-d). They have been compared with numerical simulations performed by integrating the Ikeda map model (Eq. 1 and 2). Numerical simulations have been carried out using a square pulse pump of 1 ns as in experiments, adding a low random noise. In the case of Turing instabilities (lower-branch of the bistable cycle), we used a CW pump seeded by a monochromatic signal located at the maximum gain frequency. For such large normalized cavity detuning values, the area of instability on the lower-branch is very restricted and thus very sensitive to perturbations. Consequently, seeding the system with noise should lead to unexpected switches over the upper-branch and avoid the observation of a stable temporal patterns over a large round-trip number (typically 1000 in numerical simulations). In experiments, for the sake of clarity we restricted our results to 8 round-trips but we have been able to record this steady-state over more than 30 round-trips.

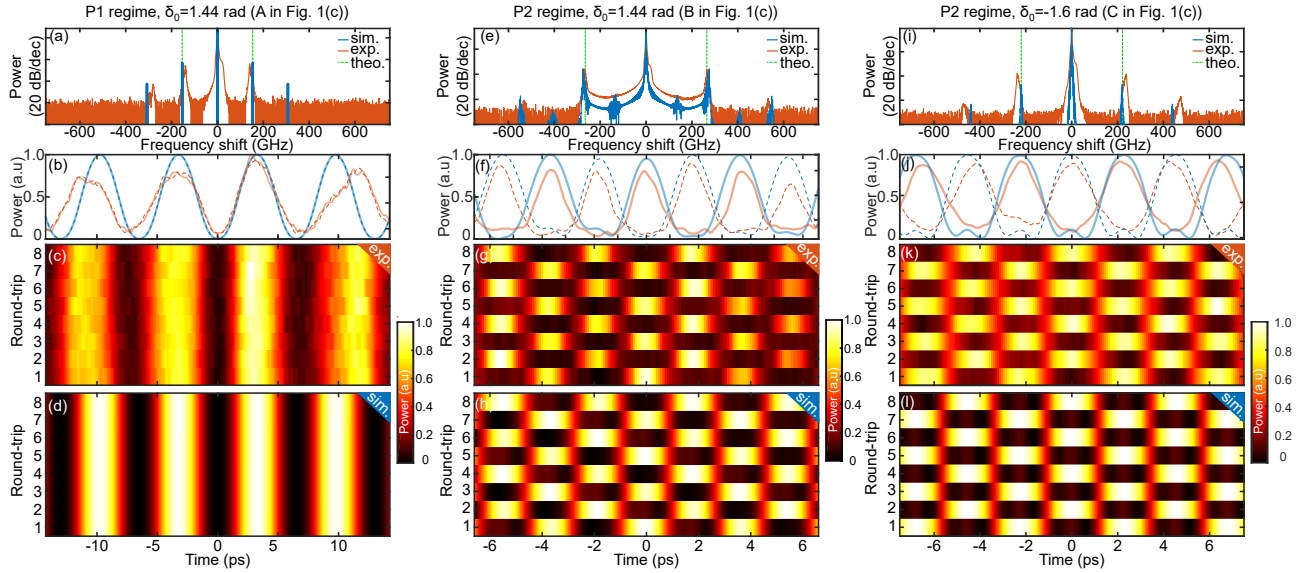

FIG. 4. (a)-(d) related to A point, (e)-(h) to B point and (i)-(l) to C point in Fig. 1(c). (a), (e) and (i) output spectra, from experiment (orange lines) and simulations (blue lines), green dashed vertical lines: theoretical sidebands positions. (b), (f) and (j) two last consecutive traces from experiment (orange lines) and simulation (blue lines). 2D-color plot of temporal traces for 8 consecutive round-trips in experiments ((c), (g) and (k)) and in numerics ((d), (h) and (l)). Cavity parameters are listed in caption of Fig. 1.

1. *Uniform cavity*

All experimental parameters are listed in the caption of Fig. 1. We investigated the configurations corresponding to points A, B and C in Fig. 1(c). First, we start by working on positive detuning to reach first P1 regime tongue on Fig. 1 by increasing the input-power. It corresponds to the configuration marked by the A point in Fig. 1(c) ($\delta_0 = 1.44$ rad and $P = 1.56$ W). Two weak side bands, symmetric around the pump are destabilized, as can be seen in Fig. 4(a). They are located at 140 GHz in really good agreement with theory predicting 154 GHz (calculated from Eq. (3) and marked by vertical dashed lines in Fig. 4(a)). The temporal pattern recorded for 8 consecutive round-trips is shown in a 2D-color plot in Fig. 4(c) where the minimum and the maximum are normalized to 0 and 1, respectively. We can note that this pulse train reproduces identical to itself round-trip to round-trip. The two last consecutive round-trip traces depicted in Fig. 4(b) (orange lines) show a quasi-perfect overlap. Thus, it proves that the system operates in the P1 regime, as expected from theory. These results are confirmed by numerical simulations with an excellent agreement for the spectrum displayed in Fig. 4 (a) (blue lines) as well as for temporal traces depicted in Fig. 4(d)-(b) corresponding respectively to 2D-color plot from intra-cavity temporal signals and two last consecutive round-trip traces from (d). For the sake of clarity, we used the same normalization than in experiments.

To reach the B point of Fig. 1(c), we increased the input-power until switching on the upper-branch where the system also features an instability zone (Fig. 1(d)). First, we observe a chaotic temporal pattern in good agreement with numerical simulations predictions (not shown here). Then, we slowly decreased it until the intra-cavity power reaches $P = 5.84$ W (input-power of 6.0 W) where the temporal waveform becomes periodic again. This is the usual way to reach operating points located close to the knee of the steady-state curve of the upper-branch. Results are depicted in Figs. 4 (e) to (h), similarly to the previous case. Two symmetric sidebands appear around the pump in the output spectrum at 273 GHz, in excellent agreement with theoretical predictions (265 GHz calculated from Eq. (3) and marked by vertical dashed lines in Fig. 4(e)) and with numerical simulations (blue lines). The normalized temporal traces obtained here alternate between two π out of phase modulated patterns at each round-trip with a singular form of a chessboard (Fig. 4(g)), that is also clear looking at the two last round-trips depicted in Fig. 4(f) (orange lines). The system undergoes P2 regime as predicted by theory. Experimental results are in excellent agreement with numerical simulations (blue lines in Fig. 4 (e) and (f) and in Fig. 4(h) corresponding to 2D-color plot from intra-cavity temporal signals) in this example too. Finally, we changed the cavity detuning to negative value $\delta_0 = -1.6$ rad, to reach first P2 regime tongue by increasing the input-power (marked by C point in Fig. 1 (c), (d)). The cavity threshold is about two times larger in that case ($P_{in} = 16.3$ W, respectively $P = 0.83$ W) compared to positive detuning cases investigated previously. Results are shown in Fig. 4 (i) to (l). Two symmetric sidebands appear around the pump at 238 GHz, in excellent agreement with theoretical predictions (221 GHz according to theoretical predictions using Eq. (3) and marked by vertical dashed lines in Fig. 4(i)) and with numeri-

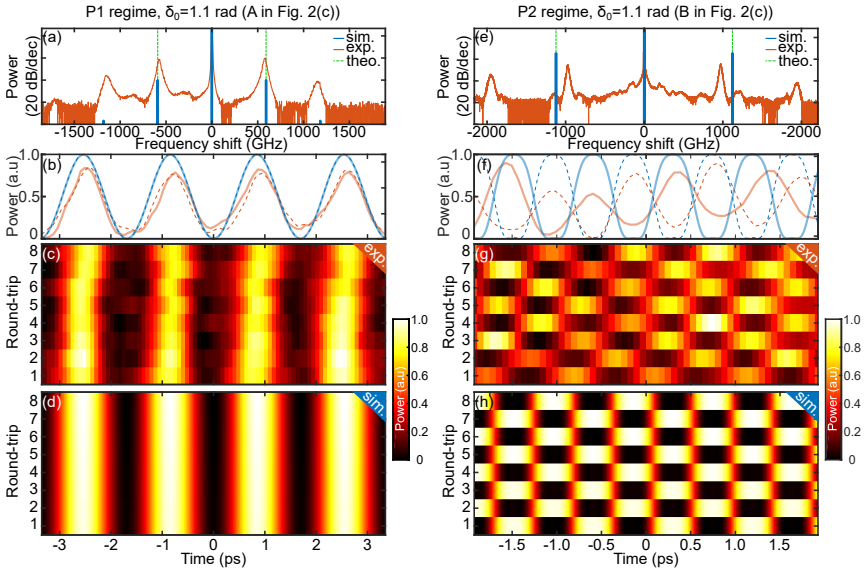

FIG. 5. (a)-(d) related to A point, (e)-(h) to B point in Fig. 2(c). (a) and (e) output spectra, from experiment (orange lines) and simulations (blue lines), green dashed vertical lines: theoretical sidebands positions. (b) and (f) two last consecutive traces from experiment (rcorange lines) and simulation (blue lines). 2D-color plot of temporal traces for 8 consecutive round-trips in experiments ((c) and(g)) and numerical simulations ((d) and (h)). Parameters are listed in Figs. 2's captions.

cal simulations (blue lines). The chessboard pattern in Fig. 4(k) clearly proves that the system undergoes a P2 regime, as expected from theory and in good agreement with numerical simulations (Fig. 4(l) and blue lines in Figs. 4 (i) and (j)).

As in the positive detuning case, we could increase the input-power to switch the system in another instability area where the temporal waveform undergoes P1 regime but this larger amount of power couldn't be reached with our experimental system.

2. *Dispersion modulated fiber cavities*

We now investigate the dispersion modulated cavity which parameters are listed in the caption of Fig. 2. The average dispersion is positive so the system is know to be modulationaly unstable if it operates in the bistable regime from LLE model. Turing instability only depends on the average dispersion value and can be observed on the lower-branch provided that the normalized detuning is larger than 4.25 [50]. Faraday instability originates from the periodic variation of the dispersion and exist on the upper-branch of the system [19, 27]. We choose to study the simplest configuration for which the period of modulation of the dispersion is equal to the cavity length ($N = 1$). Except the cavity, the experimental setup is identical to the one used in the previous section to investigate the uniform cavity. We remind that in dispersion modulated cavities, P1 and P2 regimes are respectively associated to Turing and Faraday instabilities, as it has been shown theoretically [20]. Turing and Faraday instabilities are easily discriminated in the frequency domain [19, 21, 27], and thus P1 and P2 regimes. However, analysis does not provide a direct observation of these regimes. Here we aim at performing a direct observation in the time domain and to check experimentally that P1 is associated with Turing and P2 with Faraday instabilities.

We set the cavity detuning to $\delta_0 = 1.1$ rad ($\Delta = 7$) to observe both regimes. Just above the Turing instability threshold ($P_{in} = 5.95$ W, $P = 1.14$ W), two symmetrical side bands around the pump are generated (see Fig. 5(a)). They are located at 580 GHz in really good agreement with theory predicting 591 GHz (calculated from Eq. (3) and marked by vertical dashed lines in Fig. 5(a)). Increasing the input-power up to 6.42 W ($P = 5.27$ W), the system switches onto the upper-branch of the steady-state cycle and thus Faraday instability is excited. As expected from theory [18], their spectral positions are different from Turing ones. We measured 975 GHz in experiments, which is slightly different from theory giving 1.122 THz (from Eq. (3), see vertical dashed lines in Fig. 5(e)). This discrepancy can be explain from the sensitivity of sidebands frequencies to experimental parameters in this instability domain, particularly to the intra-cavity power which is indirectly measured from the input-power. Numerical simulations represented in blue lines in Figs. 5(a) for Turing instability are in good agreement with experimental recordings (orange lines) while Fig. 5(e) for Faraday instability shows this small disagreement. Experimental temporal traces are shown in Figs. 5 (b)-(c) and (f)-(g) respectively for Turing and Faraday instabilities where corresponding numerical simulations (Figs. 5 (b), blue lines, (d) and (f), blue lines, (h)) show the same behavior. From these figures, it is clear that Turing instability lies in the P1 regime and Faraday instability in the P2 regime, and this, in excellent agreement with

numerical simulations.

IV. CONCLUSION

Real time characterization with a resolution of the order of hundreds of femtosecond allowed by time lens systems revolutionizes the way of investigating passive resonators for cavity soliton characterization [4] or in lasers for real time characterization of mode locking dynamics [40] in phase and intensity. In this work, we show that it can also be of great interest in the context of modulation instability. We anticipate that these time lens systems or more recently dual-frequency combs systems [51] will become a standard in future experiments to get real-time recordings with high resolution to improve the understanding of the complex dynamics occurring in these nonlinear systems.

V. ACKNOWLEDGMENTS

This work was partly supported by the Agence Nationale de la Recherche through the Labex Centre Europeen pour les Mathematiques, la Physique et leurs Interactions (CEMPI) and Equipex Fibres optiques pour les hauts flux (FLUX) through the "Programme Investissements d'Avenir", by the Ministry of Higher Education and Research, Hauts de France council and European Regional Development Fund (ERDF) through the Contrat de Projets Etat-Region (CPER Photonics for Society, P4S) and FEDER through the HEAFISY project.

[1] T. J. Kippenberg, A. L. Gaeta, M. Lipson, and M. L. Gorodetsky, *Dissipative Kerr solitons in optical microresonators*, Science, **361**, 6402 (2018).

[2] A. Pasquazi, M. Peccianti, L. Razzari, D.J. Moss, S. Coen, M. Erkintalo, Y.K. Chembo, T. Hansson, S. Wabnitz, P. Del'Haye, X. Xue, A.M. Weiner, and R. Morandotti, *Micro-combs: A novel generation of optical sources. Physics Reports, Micro-combs: A novel generation of optical sources*, 729, 1–81,(2018).

[3] F. Leo, S. Coen, P. Kockaert, S.-P. Gorza, P. Emplit, and M. Haelterman, *Temporal cavity solitons in one-dimensional Kerr media as bits in an all-optical buffer*, Nat. Photonics, **4**, 471 (2010).

[4] T. Herr, V. Brasch, J.D. Jost, C.Y. Wang, N.M. Kondratiev, M.L. Gorodetsky, and T.J. Kippenberg, *Temporal solitons in optical microresonators*, Nat Photon, **8**, 145-152, (2014).

[5] L. A. Lugiato and R. Lefever, *Spatial Dissipative Structures in Passive Optical Systems*, Phys. Rev. Lett., **58**, 2209 (1987).

[6] M. Haelterman, S. Trillo, and S. Wabnitz *Dissipative modulation instability in a nonlinear dispersive ring cavity*, Opt. Commun. **79**, 401–407 (1997).

[7] P. Del'Haye, T. Herr, E. Gavartin, M.L. Gorodetsky, R. Holzwarth, and T.J. Kippenberg, *Octave Spanning Tunable Frequency Comb from a Microresonator*, Phys. Rev. Lett. 107, 063901, (2011).

[8] T. Hansson, D. Modotto, and S. Wabnitz, *Dynamics of the modulational instability in microresonator frequency combs*, Phys. Rev. A **88**, 023819,(2013).

[9] S. Coen and M. Haelterman, *Modulational Instability Induced by Cavity Boundary Conditions in a Normally Dispersive Optical Fiber*, Phys. Rev. Lett., **79**, 4139 (1997).

[10] F. Leo, A. Mussot, P. Kockaert, P. Emplit, M. Haelterman, and M. Taki, *Nonlinear Symmetry Breaking Induced by Third-Order Dispersion in Optical Fiber Cavities*, Phys. Rev. Lett. **110**, 104103, 2013.

[11] A. Mussot, E. Louvergneaux, N. Akhmediev, F. Reynaud, L. Delage, and M. Taki, *Optical Fiber Systems Are Convectively Unstable*. Phys. Rev. Lett., **101**, 113904, (2008).

[12] F. Bessin, F. Copie, M. Conforti, A. Kudlinski, and A. Mussot, *Modulation instability in the weak normal dispersion region of passive fiber ring cavities*, Opt. Lett., **42**, 3730 (2017).

[13] M. Anderson, Y. Wang, F. Leo, S. Coen, M. Erkintalo, and S.G. Murdoch, *Coexistence of Multiple Nonlinear States in a Tristable Passive Kerr Resonator*, Phys. Rev. X, **7**, 031031, (2017).

[14] T. Hansson, and S. Wabnitz, *Frequency comb generation beyond the Lugiato–Lefever equation: multi-stability and super cavity solitons*, J. Opt. Soc. Am. B, **32**, 1259,(2015).

[15] M. Conforti and F. Biancalana, *Multi-resonant Lugiato-Lefever model*, Opt. Lett., **42**, 18, 3666-3669, (2017).

[16] T. Hansson, M. Bernard, and S. Wabnitz, *Modulational instability of nonlinear polarization mode coupling in microresonators*, J. Opt. Soc. Am. B, **35**, 835–841, (2018).

[17] J. Fatome, B. Kibler, F. Leo, A. Bendahmane, G.-L Oppo, B. Garbin, Y. Wang, S. G. Murdoch, M. Erkintalo, and S. Coen, *Polarization modulation instability in a fiber Kerr resonator*, Advanced Photonics 2018.

[18] M. Conforti, A. Mussot, A. Kudlinski, and S. Trillo, *Modulational instability in dispersion oscillating fiber ring cavities*, Opt. Lett., **39**, 4200 (2014).

[19] F. Copie, M. Conforti, A. Kudlinski, A. Mussot, and S. Trillo, *Competing Turing and Faraday Instabilities in Longitudinally Modulated Passive Resonators*, Phys. Rev. Lett., **116**, 143901 (2016).

[20] M. Conforti, F. Copie, A. Mussot, A. Kudlinski, and S. Trillo, *Parametric instabilities in modulated fiber ring cavities*, Opt. Lett., **41**, 5027 (2016).

[21] F. Copie, M. Conforti, A. Kudlinski, S. Trillo, and A. Mussot, *Modulation instability in the weak dispersion regime of a dispersion modulated passive fiber-ring cavity*, Opt. Express, **25**, 11283 (2017).

[22] K. Staliunas, C. Hang, and V. V. Konotop, *Parametric patterns in optical fiber ring nonlinear resonators*, Phys. Rev. A, **88**, 023846 (2013).

[23] M. Haelterman, *Simple model for the study of period-doubling instabilities in the nonlinear ring cavity*, Appl. Phys. Lett., **61**, 2756 (1992).

[24] A. Ankiewicz, and C. Pask, *Chaos in optics: field fluctuations for a nonlinear optical fibre loop closed by a coupler*, The ANZIAM Journal, **29**, 1-20 (1987).

[25] M. Haelterman, *Ikeda instability and transverse effects in nonlinear ring resonators*, Opt. Commun., **100**, 389 (1993).

[26] S. Coen, M. Haelterman, P. Emplit, L. Delage, L. M. Simohamed, and F. Reynaud, *Experimental investigation of the dynamics of a stabilized nonlinear fiber ring resonator*, JOSA B, **15**, 2283 (1998).

[27] F. Copie, M. Conforti, A. Kudlinski, S. Trillo, and A. Mussot, *Dynamics of Turing and Faraday instabilities in a longitudinally modulated fiber-ring cavity*, Opt. Lett., **42**, 435 (2017).

[28] K. Ikeda, and O. Akimoto, *Instability Leading to Periodic and Chaotic Self-Pulsations in a Bistable Optical Cavity*, Phys. Rev. Lett., **48**, 617 (1982).

[29] G. Steinmeyer, D. Jaspert, et F. Mitschke, *Observation of a period-doubling sequence in a nonlinear optical fiber ring cavity near zero dispersion*, Opt. Commun., **104**, 379 (1994).

[30] M. Nakazawa, K. Suzuki, and H. A. Haus, *Modulational instability oscillation in nonlinear dispersive ring cavity*, Phys. Rev. A **38**, 5193 (1988).

[31] R. Vallée, *Temporal instabilities in the output of an all-fiber ring cavity*, Optics Communications **81**, 419–426,(1991).

[32] N. Akhmediev, J.M. Soto-Crespo,and G. Town, *Pulsating solitons, chaotic solitons, period doubling, and pulse coexistence in mode-locked lasers: Complex Ginzburg-Landau equation approach*, Phys. Rev. E **63**, 056602, (2001).

[33] S. Boscolo, S. K. Turitsyn, and C. Finot, *Amplifier similariton fiber laser with nonlinear spectral compression*, Opt. Lett.,**37** , 4531-4533 (2012).

[34] L. Feng, P. K. A. Wai, and J. N. Kutz, J. Opt. Soc. Am. B,*Geometrical description of the onset of multi-pulsing in mode-locked laser cavities*, **27**, 2068 (2010).

[35] L. Luo, T.J. Tee, and P.L. Chu, *Chaotic behavior in erbium-doped fiber-ring lasers*, J. Opt. Soc. Am. B, **15**, 972–978, (1998).

[36] G. Sucha, S. R. Bolton, S. Weiss, and D. S. Chemla, *Period doubling and quasi-periodicity in additive-pulse mode-locked lasers*, Opt. Lett., **20**, 1794-1796 (1995).

[37] R. Salem, M. A. Foster, and A. L. Gaeta, *Application of space-time duality to ultrahigh-speed optical signal processing*, Adv. Opt. Photonics, **5**, 274 (2013).

[38] P. Suret, R.E. Koussaifi, A. Alexey, C. Evain, S. Randoux, S. Szwaj, and S. Bielawski, *Single-shot observation of optical rogue waves in integrable turbulence using time microscopy*, Nat. Commun., **7**, 13136 (2016).

[39] M. Närhi , B. Wetzel, C. Billet, S. Toenger, T. Sylvestre, J.-M Merolla, R. Morandotti, F. Dias, G. Genty, and J.M. Dudlet, *Real-time measurements of spontaneous breathers and rogue wave events in optical fibre modulation instability*, Nat. Commun., **7**, 13675 (2016).

[40] P. Ryczkowski, M. Närhi, C. Billet, J.-M. Merolla, G. Genty, and J. M. Dudley, *Real-time full-field characterization of transient dissipative soliton dynamics in a mode-locked laser*, Nat. Photonics, **12**, 221 (2018).

[41] B. H. Kolner and M. Nazarathy, *Temporal imaging with a time lens*, Opt. Lett., **14**, 630 (1989).

[42] D. W. McLaughlin, J. V. Moloney, and A. C. Newell, *New Class of Instabilities in Passive Optical Cavities*, Phys. Rev. Lett., **54**, 681 (1985).

[43] S. Coen and M. Haelterman, *Competition between modulational instability and switching in optical bistability*, Opt. Lett., **24**, 80 (1999).

[44] S. Coen, M. Haelterman, P. Emplit, L. Delage, L. M. Simohamed, and François Reynaud, *Bistable switching induced by modulational instability in a normally dispersive all-fibre ring cavity*, J. Opt. B Quantum Semiclassical Opt., **1**, 36 (1999).

[45] A. Mussot, M. Conforti, S. Trillo, F. Copie, and A. Kudlinski, *Modulation instability in dispersion oscillating fibers*, Adv. Opt. Photon., **10**, 1-42 (2018).

[46] N. Tarasov, A. M. Perego, D. V. Churkin, K. Staliunas, and S. K. Turitsyn, *Mode-locking via dissipative Faraday instability*, Nature Communications, **7**, 12441 (2016).

[47] F. Copie, M. Conforti, A. Kudlinski, A. Mussot, F. Biancalana, and S. Trillo, *Instabilities in passive dispersion oscillating fiber ring cavities*. Europ. Phys. Journal. D **71**, (2017).

[48] S.-W. Huang, A. K. Vinod, J. Yang, M. Yu, D.-L. Kwong, and C. W. Wong, *Quasi-phase-matched multispectral Kerr frequency comb*, Opt. Lett., **42**, 2110-2113 (2017).

[49] Lin, A.L., Bertram, M., Martinez, K., Swinney, H.L., Ardelea, A., and Carey, G.F., *Resonant phase patterns in a reaction-diffusion system*, Phys. Rev. Lett. **84**, 4240, (2000).

[50] S. Coen and M. Haelterman, *Continuous-wave ultrahigh-repetition-rate pulse-train generation through modulational instability in a passive fiber cavity*, Opt. Lett., **26**, 39 (2001).

[51] X. Yi, Q.-F. Yang, K. Y. Yang, and K. Vahala, *Imaging soliton dynamics in optical microcavities*, Nature Communications 9, 3565 (2018).